


## Anionic electron dimensionality and monolayer ferromagnetism in Y-Co electrides

Lu Zheng(郑璐), Zimeng Lv(吕梓萌), Xiaochen Huang(黄小琛), Zhuangfei Zhang(张壮飞), Chao Fang(房超), Yuewen Zhang(张跃文), Qianqian Wang(王倩倩), Liangchao Chen(陈良超), Xiaopeng Jia(贾晓鹏), Biao Wan(万彪), and Huiyang Gou(缑慧阳)

**Citatio:**Chin. Phys. B, 2025, 34 (**9**): 097105. DOI: 10.1088/1674-1056/adf82f
http://cpb.iphy.ac.cn; http://iopscience.iop.org/cpb

**What follows is a list of articles you may be interested in**

---

## Momentum-dependent anisotropy of the charge density wave gap in quasi-1D $ZrTe_{3-x}Se_x$ ($x$ = 0.015)

Renjie Zhang(张任杰), Yudong Hu(胡裕栋), Yiwei Cheng(程以伟), Yigui Zhong(钟益桂), Xuezhi Chen(陈学智), Junqin Li(李俊琴), Kozo Okazaki, Yaobo Huang(黄耀波), Tian Shang(商恬), Shifeng Jin(金士锋), Baiqing Lv(吕佰晴), and Hong Ding(丁洪)

Chin. Phys. B, 2025, 34 (**7**): 077106. DOI: 10.1088/1674-1056/addcc5

## Angle-resolved photoemission spectroscopy study on transition-metal kagome materials

Jiangang Yang(杨鉴刚), Jianwei Huang(黄建伟), Lin Zhao(赵林), and X. J. Zhou(周兴江)

Chin. Phys. B, 2025, 34 (**4**): 047101. DOI: 10.1088/1674-1056/adb689

## Effects of vacancy and external electric field on the electronic properties of the $MoSi_2N_4$/graphene heterostructure

Qian Liang(梁前), Xiangyan Luo(罗祥燕), Guolin Qian(钱国林), Yuanfan Wang(王远帆), Yongchao Liang(梁永超), and Quan Xie(谢泉)

Chin. Phys. B, 2024, 33 (**3**): 037101. DOI: 10.1088/1674-1056/acef04

## Investigation of electronic, elastic, and optical properties of topological electride $Ca_3Pb$ via first-principles calculations

Chang Sun(孙畅), Xin-Yu Cao(曹新宇), Xi-Hui Wang(王西惠), Xiao-Le Qiu(邱潇乐), Zheng-Hui Fang(方铮辉), Yu-Jie Yuan(袁宇杰), Kai Liu(刘凯), and Xiao Zhang(张晓)

Chin. Phys. B, 2021, 30 (**5**): 057104. DOI: 10.1088/1674-1056/abec38

## Electronic structure of O-doped SiGe calculated by DFT+$U$ method

Zong-Yan Zhao(赵宗彦), Wen Yang(杨雯), Pei-Zhi Yang(杨培志)

Chin. Phys. B, 2016, 25 (**12**): 127101. DOI: 10.1088/1674-1056/25/12/127101

---

**SPECIAL TOPIC — Structures and properties of materials under high pressure**

# Anionic electron dimensionality and monolayer ferromagnetism in Y–Co electrides

Lu Zheng(郑璐)[1], Zimeng Lv(吕梓萌)[1], Xiaochen Huang(黄小琛)[1], Zhuangfei Zhang(张壮飞)[1], Chao Fang(房超)[1], Yuewen Zhang(张跃文)[1], Qianqian Wang(王倩倩)[1], Liangchao Chen(陈良超)[1], Xiaopeng Jia(贾晓鹏)[2], Biao Wan(万彪)[1,†], and Huiyang Gou(缑慧阳)[3]

[1] *Key Laboratory of Material Physics of Ministry of Education, School of Physics and Laboratory of Zhongyuan Light, Zhengzhou University, Zhengzhou* 450052, *China*

[2] *State Key Laboratory of High Pressure and Superhard Materials, Jilin University, Changchun* 130012, *China*

[3] *Center for High Pressure Science and Technology Advanced Research, Beijing* 100094, *China*

(Received 7 July 2025; revised manuscript received 1 August 2025; accepted manuscript online 6 August 2025)

Electrides, characterized by spatially confined anionic electrons, have emerged as a promising class of materials for catalysis, magnetism, and superconductivity. However, transition-metal-based electrides with diverse electron dimensionalities remain largely unexplored. Here, we perform a comprehensive first-principles investigation of Y–Co electrides, focusing on $Y_3Co$, $Y_3Co_2$, and YCo. Our calculations reveal a striking dimensional evolution of anionic electrons: from two-dimensional (2D) confinement in YCo to one-dimensional (1D) in $Y_3Co_2$ and zero-dimensional (0D) in $Y_3Co$. Remarkably, the YCo monolayer exhibits intrinsic ferromagnetism, with a magnetic moment of 0.65 $\mu_B$ per formula unit arising from spin-polarized anionic electrons mediating long-range coupling between Y and Co ions. The monolayer also shows a low exfoliation energy (1.66 J/m$^2$), indicating experimental feasibility. All three electrides exhibit low work functions (2.76 eV–3.11 eV) along with Co-centered anionic states. This work expands the family of transition-metal-based electrides and highlights dimensionality engineering as a powerful strategy for tuning electronic and magnetic properties.

**Keywords:** electrides, cobalt anions, work function, magnestism

**PACS:** 71.20.–b, 73.22.–f, 62.50.–p, 31.15.A–

**DOI:** 10.1088/1674-1056/adf82f **CSTR:** 32038.14.CPB.adf82f

## 1. Introduction

Rare-earth (*Re*) element–transition metal (TM) compounds have long been central to research in magnetism, catalysis, and hydrogen storage, attracting considerable attention over the past few decades.[1–3] Although diverse *Re*-rich *Re*-TM compounds have been synthesized, many have received limited attention due to their weak or negligible magnetic properties. Recent studies, however, reveal that in these *Re*-rich systems, itinerant electrons can localize within the atomic voids of rare-earth atoms, acting as anionic species, commonly referred to as anionic electrons. These materials, known as electrides, have since emerged as important candidates for applications in catalytic energy conversion, electron injection technologies, and superconductivity, inspiring renewed cross-disciplinary scientific interest.[4–10]

Anionic electrons in electrides are characterized by weak binding energies and ultra-low effective masses, which give rise to exceptional physical properties such as enhanced quantum confinement, high carrier mobility, and low work functions.[11–13] Recent research has focused on discovering new electride materials and tuning their emergent functionalities for advanced electronic and energy applications. Notable examples include $Ca_2N$[14,15] and C12A7[16], which exhibit ultra-low work functions of 2.6 eV and 2.4 eV, respectively. These materials are widely used as efficient electron injection layers in organic light-emitting diodes (OLEDs), improving charge transport and device performance.[17] Beyond their charge properties, anionic electrons can also display spin polarization and strong interactions with neighboring atoms, as seen in Mott-insulating $Ba_5Sb_3$[18] and antiferromagnetic $Ba_3MnN_3$.[4] Transition metals have also been shown to carry negative charges, forming intermetallic electrides with electropositive metals.[19–21] Owing to their chemical stability, phase diversity, and multifunctionality, transition-metal electrides have become a major focus in recent materials research. Their low work functions, combined with the presence of transition metals, enable effective electron transfer to adsorbed molecules, leading to high catalytic performance in chemoselective hydrogenation reactions, exemplified by compounds such as $Y_3Pd_2$,[5] $YRu_2$,[20] and $LaCu_{0.67}Si_{1.33}$.[22] Additionally, superconducting electrides like $Nb_5Ir_3$[23] and $Li_8Au$[24] have been discovered, featuring transition metal anions. The d orbitals in these materials modulate the topology of electron cavities, predominantly forming zero-dimensional (0D)

[†]Corresponding author. E-mail: biaowan@zzu.edu.cn

© 2025 Chinese Physical Society and IOP Publishing Ltd. All rights, including for text and data mining, AI training, and similar technologies, are reserved.

states or one-dimensional (1D) channels. Recently, BaCu was identified as a two-dimensional (2D) electride with copper anions.[19,25] BaCu not only retains the advantageous properties of conventional ionic 2D electrides but also exhibits unique features such as nearly isotropic physical behavior and highly delocalized anionic electrons. This diversity underscores the scientific and technological significance of exploring new transition-metal electrides.

The yttrium–cobalt (Y–Co) system exemplifies phase diversity and multifunctionality. For example, $YCo_5$ and $Y_2Co_{17}$ have shown promise in electromagnetic applications.[26,27] In 2015, ferromagnetism and superconductivity were observed to coexist in the Y-rich compound $Y_9Co_7$, where the magnetism arises from itinerant electrons rather than Co atoms.[28] Nevertheless, the lack of atomic voids in $Y_9Co_7$ restricts the formation of anionic electrons. Nevertheless, the high density of itinerant electrons indicates potential electride behavior in the Y–Co system, offering an attractive platform to explore novel transition-metal electrides. In this study, structural analysis combined with comprehensive theoretical calculations confirms that $Y_3Co$, $Y_3Co_2$, and YCo exhibit 0D, 1D, and 2D electride characteristics, respectively. Their low work functions and the presence of Co anions highlight their potential for catalytic and optoelectronic applications. Notably, the YCo monolayer displays a low exfoliation energy alongside ferromagnetic behavior, where spin-polarized anionic electrons mediate long-range magnetic coupling between yttrium and cobalt ions.

## 2. Methods

The crystal structures of YCo,[29] $Y_3Co_2$[30], and $Y_3Co$[31] were obtained from the inorganic crystal structure database (ICSD). First-principles calculations were performed using the Vienna *Ab initio* Simulation Package (VASP),[32] employing the generalized gradient approximation (GGA) with the Perdew–Burke–Ernzerhof (PBE) functional in combination with the projector-augmented wave (PAW) method to describe the electronic structure.[33,34] A plane-wave cutoff of 500 eV and a Monkhorst-Pack $k$-point grid with a density parameter of $2\pi \times 0.03$ Å$^{-1}$ were employed to ensure convergence. For a more accurate description of the structural and electronic properties of YCo, the van der Waals density functional (vdW-DF) with the optB86b functional was applied.[35] Spin-polarized calculations indicate that YCo, $Y_3Co_2$, and $Y_3Co$ exhibit nonmagnetic ground states, whereas the YCo monolayer displays intrinsic ferromagnetism. The phonon dispersion curves of the YCo monolayer were computed using the PHONOPY package within the finite-displacement method framework.[36]

Work functions were systematically calculated for YCo along the (001) and (110) surfaces, $Y_3Co_2$ along the (001) and (010) surfaces, and $Y_3Co$ along the (001), (010), and (100) surfaces. The work function values were determined using the following formula:

$$\Phi_{\mathrm{WF}} = E_{\mathrm{vac}} - E_{\mathrm{f}}, \tag{1}$$

where $E_{\mathrm{vac}}$ and $E_{\mathrm{f}}$ represent the vacuum energy level and the Fermi level of the system, respectively.

For the YCo monolayer calculations, a vacuum layer with a thickness of 16 Å was employed to prevent spurious interactions between periodic slabs. The exfoliation energy ($\Delta E_{\mathrm{exf}}$) of the YCo monolayer was computed via the following equation:[37,38]

$$\Delta E_{\mathrm{exf}} = \frac{E_{\mathrm{2D}} - \frac{1}{m}E_{\mathrm{bulk}}}{A}. \tag{2}$$

Here, $E_{\mathrm{2D}}$ and $E_{\mathrm{bulk}}$ denote the total energies of the fully optimized monolayer and bulk YCo structures, respectively, while $A$ represents the in-plane surface area of the monolayer unit cell. Here, $m = 3$ corresponds to the number of layers within the bulk crystal model.

## 3. Results and discussion

### 3.1. Structure analysis

The valence electron concentration and cavity topology are key factors governing electride formation. In rare-earth-containing electrides, anionic electrons are typically confined within F-center voids created by $Re_6$ octahedrons.[39] Guided by these principles, we investigate three electron-rich Y–Co compounds (YCo, $Y_3Co_2$, and $Y_3Co$), each featuring $Y_6$ octahedral lattice voids. Their crystal structures are illustrated in Fig. 1. In all three compounds, Co atoms are coordinated by six Y atoms, with Y–Co bond distances ranging from 2.86 Å–2.88 Å in YCo, 2.75 Å–2.86 Å in $Y_3Co$, and 2.79 Å–2.96 Å in $Y_3Co_2$.

YCo adopts a trigonal structure (space group $R$-3$m$, Fig. 1(a)), notable for its distinct layered arrangement despite all constituents being metallic. The interlayer spacing in YCo is 3.24 Å, comparable to that of the 2D electride $Y_2C$ (3.20 Å).[40] In YCo, Co atoms form a unique in-plane honeycomb network ($d_{\mathrm{Co-Co}} = 2.25$ Å), reminiscent of the Cu–Cu honeycomb lattice found in the 2D intermetallic electride BaCu.[19] Edge-sharing $Y_6$ octahedra in YCo generate 2D interlayer voids perpendicular to the $c$-axis.

$Y_3Co_2$ (Fig. 1(b)), with higher yttrium content, crystallizes in an orthorhombic *Pnnm* structure. The increased Y fraction promotes the formation of Co–Co dimers with bond lengths of 2.40 Å–comparable to metallic Co (2.42 Å)–suggesting possible metallic bonding. Similar to $Y_5Si_3$,[41] edge-sharing $Y_6$ octahedra develop 1D channel-like voids along the $c$-axis, while top-sharing $Y_6$ octahedra contribute to the formation of 0D voids.

$Y_3Co$, the most Y-rich phase among the three, also crystallizes in the *Pnnm* structure (Fig. 1(c)). Here, the high Y content leads to full separation of Co atoms, with top-sharing $Y_6$ octahedra aligned along the *b*-axis, forming isolated 0D voids.

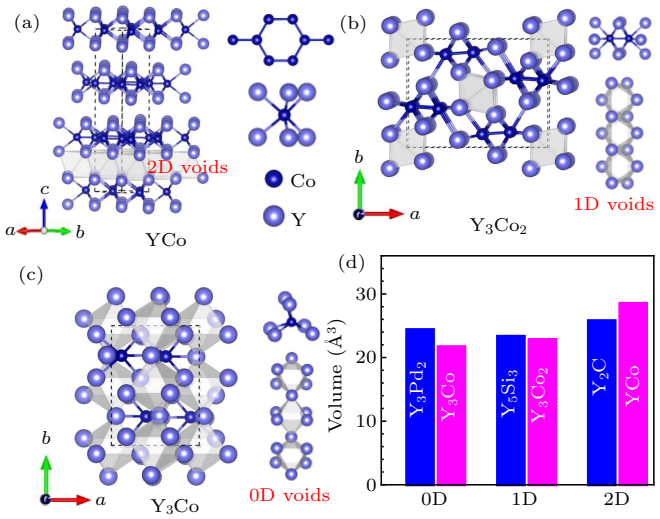



**Fig. 1.** Crystal structures of YCo (a), $Y_3Co_2$ (b), and $Y_3Co$ (c), where $Y_6$ octahedra form zero-dimensional (0D), one-dimensional (1D), and two-dimensional (2D) voids, respectively. Volume comparison of $Y_6$ octahedral voids in isodimensional Y-based electrides (d).

Cavity volume plays a decisive role in electride stabilization by allowing valence electrons from surrounding atoms to localize within these interstitial sites. To establish a structural comparison framework, we evaluate the $Y_6$ octahedral void volumes in these Y–Co compounds relative to known Y-based electrides. As shown in Fig. 1(d), the void volumes of YCo, $Y_3Co_2$, and $Y_3Co$ are comparable to those of previously reported 0D, 1D, and 2D Y-based electrides.[5,40,41] This combination of electron-rich composition and substantial interstitial space confirms that YCo, $Y_3Co_2$, and $Y_3Co$ meet the structural and electronic criteria for electride formation.

### 3.2. Identification and electronic structures of Y–Co electrides

To visualize electron distribution and confirm the presence of anionic electrons, electron localization function (ELF) calculations were performed for the Y–Co compounds. As shown in Fig. 2, highly localized ELF regions appear within the $Y_6$ octahedra of YCo (Fig. 2(a)), $Y_3Co_2$ (Fig. 2(b)), and $Y_3Co$ (Fig. 2(c)). The ELF values between these attractors and surrounding Y atoms approach zero–a hallmark of anionic electrons in electrides. In $Y_3Co$, ELF attractors within the top-shared $Y_6$ octahedra remain spatially isolated, forming a 0D distribution. By contrast, $Y_3Co_2$ and YCo exhibit interconnected ELF attractors within edge-shared $Y_6$ octahedra, resulting in 1D chain-like and 2D layered electron distributions, respectively.

Across all Y–Co compounds, ELF values between Co and Y atoms remain slightly below 0.5 (left panels of Figs. 2(d)–2(f)). This indicates the coexistence of metallic and ionic bonding. As shown in Fig. S1, Y–Co bonds in YCo, $Y_3Co_2$, and $Y_3Co$ exhibit notable anti-bonding states near the Fermi level, a phenomenon absent in $YCo_2$.[19] Such anti-bonding states facilitate the formation of anionic electrons. Additionally, ELF values near 0.5 between neighboring Co atoms in YCo and $Y_3Co_2$ (Fig. S2) suggest the presence of metallic Co–Co interactions.

To further probe charge distribution, charge density difference calculations were performed. Significant electron accumulation occurs within $Y_6$ interstitial voids (right panels of Figs. 2(d)–2(f)), reflecting electron transfer from Y atoms and confirming the presence of anionic electrons. Additional charge accumulation around Co atoms supports ionic Y–Co bonding and the existence of negatively charged

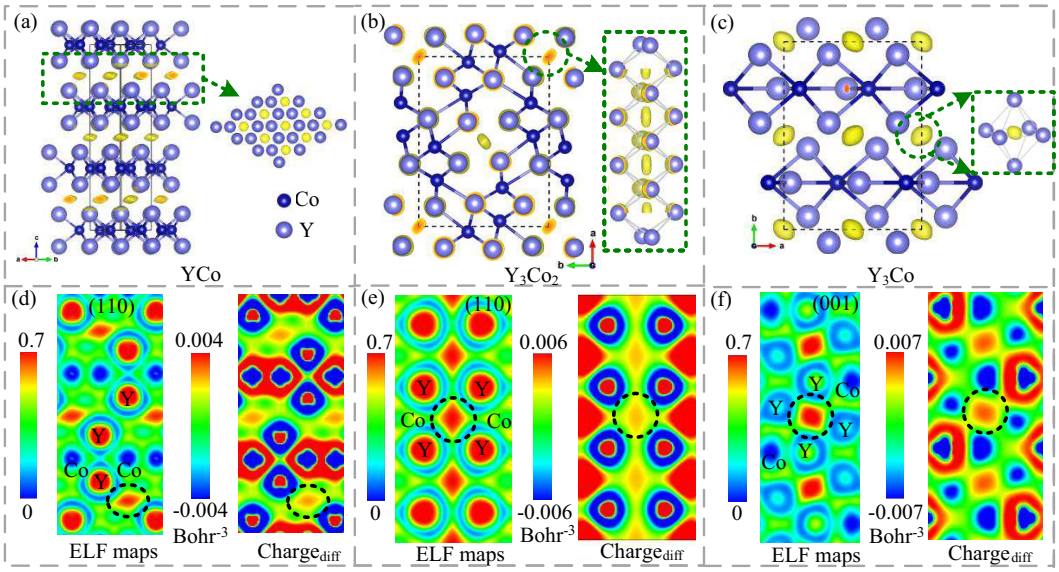



**Fig. 2.** 3D ELF maps of YCo (a), $Y_3Co_2$ (b) and $Y_3Co$ (c) with isosurfaces of 0.6, 0.6 and 0.75, respectively. 2D ELF maps (left site) and charge density difference (right site) of YCo in the (110) plane (d), $Y_3Co_2$ in (110) plane (e), and $Y_3Co$ in (001) plane (f).

Co species. Bader charge analysis reveals that each Co atom gains 1.1$e$ in YCo, 2.3e in $Y_3Co$, and 1.4–1.8 $e$ in $Y_3Co_2$. Negatively charged cobalt ions have also been reported in La-CoSi electride,[21] where they play a key role in mediating electron transfer for $N_2$ dissociation and promoting efficient ammonia synthesis.

Electronic structure calculations indicate that all three Y–Co electrides are metallic with no evidence of long-range magnetic ordering. To further characterize anionic electrons, projected band structure calculations were performed using pseudo-atoms ($r = 1.6$ Å) at the $Y_6$ octahedral voids. As shown in Figs. 3 and S3, states associated with anionic electrons in YCo (Fig. 3(a)), $Y_3Co_2$ (Fig. 3(b)), and $Y_3Co$ (Fig. 3(c)) are predominantly near the Fermi level, distinguishing them from conventional multi-center bonding states.[42] Unlike isolated energy bands in ionic electrides,[40] these anionic electron states span multiple bands, which indicates strong orbital hybridization with surrounding Y atoms, a defining feature of intermetallic electrides. Similar hybridization has been reported in $Y_5Si_3$[41] and $Yb_5Sb_3$,[43] enhancing structural stability. Band dispersion analysis reveals stronger localization of anionic electrons in $Y_3Co_2$ and $Y_3Co$ compared to YCo, highlighting the role of void dimensionality in electron confinement.

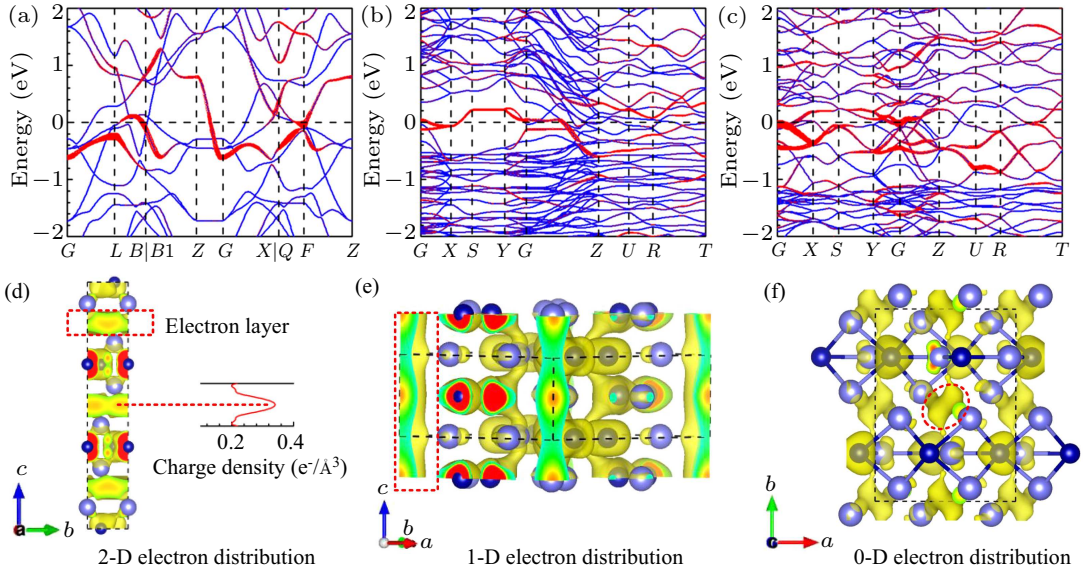



**Fig. 3.** Projected band structures of anionic electrons in YCo (a) and $Y_3Co_2$ (b) and $Y_3Co$ (c). Partial charge densities of the energy bands that are primarily occupied by anionic electrons near the Fermi level in YCo (d) and $Y_3Co_2$ (e) and $Y_3Co$ (f).

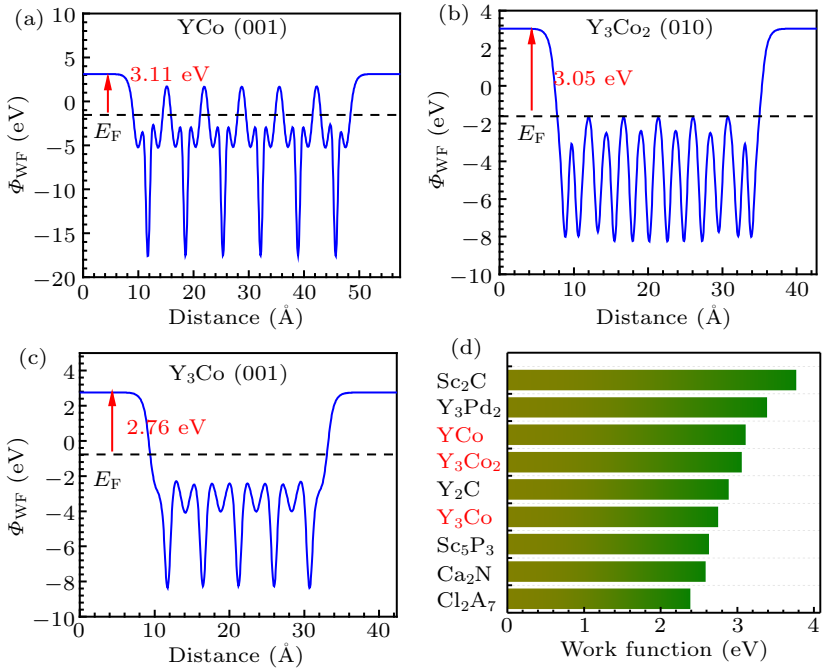



**Fig. 4.** Work function of YCo in (001) surface (a), $Y_3Co_2$ in (010) surface (b) and $Y_3Co$ in (001) surface (c). The comparison of the work function for Y-Co electrides and previously reported electrides (d).

Partial charge density analyses directly visualize the spatial distribution of anionic electrons. YCo exhibits 2D delocalized electrons in interlayer regions (Fig. 3(d)), reminiscent of BaCu,[19] where 2D anionic electrons contribute to low electrical resistivity. $Y_3Co_2$ shows 1D electron localization along the *c*-axis within tubular channels (Fig. 3(e)), consistent with 1D electrides such as $Ho_5Si_3$[44] and $Ba_3CrN_3$.[45] $Y_3Co$ exhibits 0D electron localization (Fig. 3(f)). From structural topology and electron distribution, YCo, $Y_3Co_2$, and $Y_3Co$ are thus classified as 2D, 1D, and 0D electrides, respectively. Integration of partial density of states estimates anionic electrons per void as 0.87 for YCo, 1.26 for $Y_3Co_2$, and 1.37 for $Y_3Co$. High pressure increases the charge magnitude of anionic electrons (Fig. S4), primarily due to enhanced Coulomb repulsion promoting electron transfer into lattice interstices. ELF results further indicate enhanced localization under pressure.

The weakly bound nature of anionic electrons confers low work functions and high performance in catalytic reactions and electron emission devices. Work functions of Y–Co electrides were calculated (Figs. 4 and S5), ranging from 3.12 eV to 3.21 eV for YCo, 3.07 eV to 3.62 eV for $Y_3Co_2$, and 2.76 eV to 3.32 eV for $Y_3Co$. Surface-dependent analysis shows that the (001), (010), and (100) surfaces exhibit the lowest surface energies and corresponding work functions for YCo (Fig. 4(a)), $Y_3Co_2$ (Fig. 4(b)), and $Y_3Co$ (Fig. 4(c)), respectively. Notably, $Y_3Co$ achieves the lowest work function of 2.76 eV on its (010) surface, attributable to its high density of anionic electrons. Compared with previously reported electrides (Fig. 4(d)),[5,14,16,40,46,47] the Y–Co electrides exhibit work functions comparable to other rare-earth-based electrides and slightly higher than $Ca_2N$.[14] The coexistence of intrinsic anionic Co species and ultra-low work functions (2.76–3.62 eV) highlights their potential for next-generation catalytic technologies and electron emission applications.

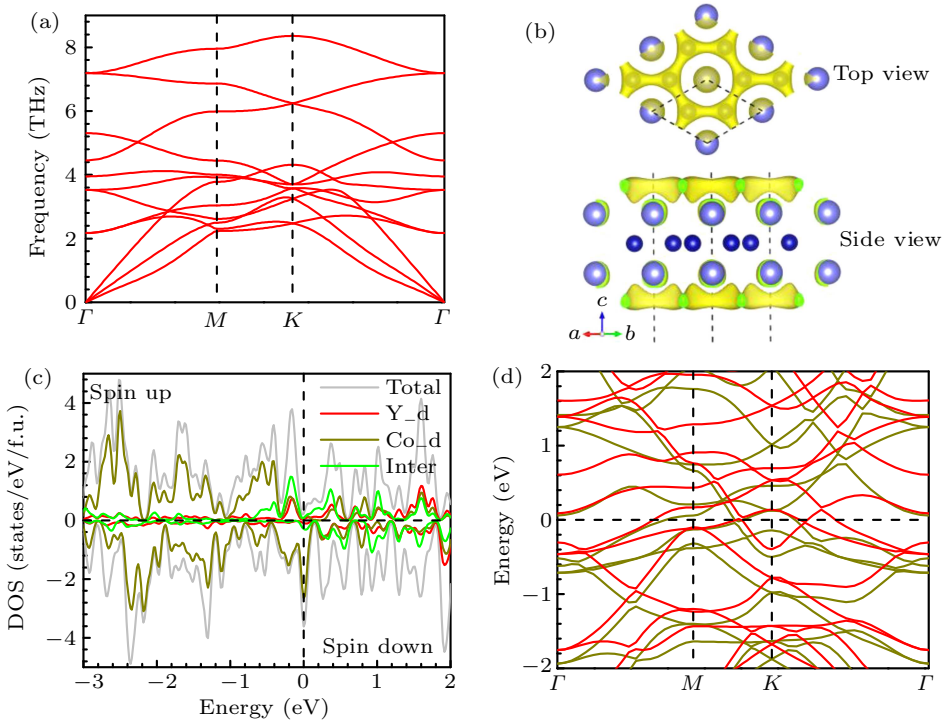



**Fig. 5.** Phonon spectra (a), electron localization function (ELF) maps (b), density of states (DOS) (c), and band structure of the YCo monolayer (d).

### 3.3. Electronic structures and magnetic properties of YCo monolayer

The rapid advancement of nanodevices has intensified the search for atomically thin materials with novel physical properties.[48–51] In 2D electrides, adjacent atomic layers are held together by interlayer anionic electrons. The weak interaction between these electrons and the atomic layers suggests that mechanical exfoliation of monolayer electrides — also called electrenes — is feasible, as experimentally demonstrated for materials such as $Ca_2N$, $Sr_2N$, and $Y_2C$,[52] which exhibit low work functions, high electrical conductivity, and exceptional carrier mobility.

The YCo monolayer exhibits a low exfoliation energy of 1.66 J/m$^2$, slightly lower than that of $Y_2C$ (1.80 J/m$^2$), suggesting that mechanical exfoliation is feasible. Phonon dispersion calculations confirm its kinetic stability, with no imaginary frequencies observed (Fig. 5(a)). ELF maps (Fig. 5(b)) indicate that the monolayer preserves its 2D electride character, with anionic electrons delocalized across surface regions. Compared to the bulk, anionic electrons in the monolayer are more delocalized (ELF isosurface: 0.35), likely due to reduced coordination of neighboring Y atoms.

Remarkably, the YCo monolayer exhibits intrinsic ferro-

magnetism with a magnetic moment of 0.65 $\mu_B$ per formula unit. This magnetism arises from spin polarization of Y/Co d-electrons and delocalized anionic electrons, as confirmed by spin-resolved density of states and magnetic moment analysis (Figs. 5(c) and 5(d)). Introducing hydrogen atoms into the interstitial voids to deplete anionic electrons completely suppresses ferromagnetism (Fig. S6), highlighting the crucial role of spin-polarized interstitial electrons in mediating long-range magnetic ordering.

The emergence of magnetism in the monolayer, absent in the bulk, is attributed to reduced orbital hybridization in the low-coordination environment of surface Y atoms. This behavior is consistent with trends observed in anti-$CdCl_2$-type rare-earth carbides ($Re_2C$, where $Re$ = Y, Gd, Tb, Dy, Ho), which exhibit paramagnetic or ferromagnetic ground states driven by spin-polarized interstitial electrons.[53] In contrast, isostructural $Sc_2C$[46] remains nonmagnetic and semiconducting due to strong hybridization between Sc atoms and interstitial electrons, which suppresses spin polarization. The pronounced spin polarization of anionic electrons near the Fermi level positions the YCo monolayer as a promising candidate for future nano-spintronic and 2D magnetic device applications.

## 4. Conclusion

In summary, our comprehensive study demonstrates that YCo, $Y_3Co_2$, and $Y_3Co$ are intermetallic electrides characterized by dimensional diversity in anionic electron distribution and the presence of anionic Co species. Notably, YCo exhibits a unique Co honeycomb lattice with metallic bonding, allowing YCo monolayers to form a distinct 2D layered structure. Anionic electrons in these compounds are confined within F-center voids formed by $Y_6$ octahedra, exhibiting 2D, 1D, and 0D spatial distributions in YCo, $Y_3Co_2$, and $Y_3Co$, respectively. Their localization and charge magnitude can be significantly tuned by pressure.

The work functions of these compounds scale with the density of anionic electrons, ranging from 3.11 eV (YCo, (001) surface) to 2.76 eV ($Y_3Co$, (010) surface). The YCo monolayer is distinguished by a low exfoliation energy (1.66 J/m$^2$) and high kinetic stability, suggesting practical feasibility for experimental exfoliation. Remarkably, while all bulk Y–Co electrides are non-magnetic, the YCo monolayer exhibits intrinsic ferromagnetism with a magnetic moment of 0.65 $\mu_B$ per formula unit, mediated by spin-polarized interstitial electrons. These findings significantly broaden the family of transition-metal-based electrides and provide theoretical guidance for designing multifunctional electrides with tunable electronic, magnetic, and catalytic properties.

## Acknowledgements

The authors acknowledge funding support from the National Science Fund for Distinguished Young Scholars (Grant No. T2225027), the National Natural Science Foundation of China (Grant Nos. 12074013 and 12204419), and the China Postdoctoral Science Foundation (Grant No. 2021M702956).

## References

[1] Yang W, Zhang Y, Qiao G, Lai Y, Liu S, Wang C, Han J, Du H, Zhang Y, Yang Y, Hou Y and Yang J 2018 *Acta Mater.* **145** 331
[2] Ma Z, Yue M, Liu H, Yin Z, Wei K, Guan H, Lin H, Shen M, An S, Wu Q and Sun S 2020 *J. Am. Chem. Soc.* **142** 8440
[3] Pandey S K, Srivastava A and Srivastava O N 2007 *Int. J. Hydrog. Energy* **32** 2461
[4] Zhang X, Meng W, Liu Y, Dai X, Liu G and Kou L 2023 *J. Am. Chem. Soc.* **145** 5523
[5] Ye T N, Lu Y, Xiao Z, Li J, Nakao T, Abe H, Niwa Y, Kitano M, Tada T and Hosono H 2019 *Nat. Commun.* **10** 5653
[6] Hosono H and Kitano M 2021 *Chem. Rev.* **121** 3121
[7] Guan X, Huo B and Chen G 2024 *Chin. Phys. B* **33** 060311
[8] Liang Y, Lin X, Wan B, Guo Z, Cao X, Shao D, Sun J and Gou H 2024 *Phys. Rev. Res.* **6** 023249
[9] Wan B, Zhang J, Wu L and Gou H 2019 *Chin. Phys. B* **28** 106201
[10] Yang Q, Jiang X and Zhao J 2023 *Chin. Phys. Lett.* **40** 107401
[11] Dye J L 2009 *Acc. Chem. Res.* **42** 1564
[12] Dye J L 1990 *Science* **247** 663
[13] Liu Y, Cui T and Li D 2025 *Matter and Radiation at Extremes* **10** 027802
[14] Lee K, Kim S W, Toda Y, Matsuishi S and Hosono H 2013 *Nature* **494** 336
[15] Wang Q, Liu K, Xue X, Zhang L, Pang R, Ren X, Zhao X and Li S 2024 *Phys. Rev. B* **109** 085420
[16] Matsuishi S, Toda Y, Miyakawa M, Hayashi K, Kamiya T, Hirano M, Tanaka I and Hosono H 2003 *Science* **301** 626
[17] Hosono H, Kim J, Toda Y, Kamiya T and Watanabe S 2017 *Proc. Natl. Acad. Sci. USA* **114** 233
[18] Xu Y, Zheng L, Zhang Y, Zhang Z, Wang Q, Zhang Y, Chen L, Fang C, Wan B and Gou H 2024 *Matter and Radiation at Extremes* **9** 037402
[19] Wan B, Yuan Y, Zheng L, Xu Y, Zhao S, Liu K, Huang D, Wu L, Zhang Z, Wang G, Li J, Zhang S and Gou H 2024 *J. Am. Chem. Soc.* **146** 17508
[20] Ogawa T, Kobayashi Y, Mizoguchi H, Kitano M, Abe H, Tada T, Toda Y, Niwa Y and Hosono H 2018 *J. Phys. Chem. C* **122** 10468
[21] Gong Y, Wu J, Kitano M, Wang J, Ye T N, Li J, Kobayashi Y, Kishida K, Abe H, Niwa Y, Yang H, Tada T and Hosono H 2018 *Nat. Catal.* **1** 178
[22] Ye T N, Lu Y, Li J, Nakao T, Yang H, Tada T, Kitano M and Hosono H 2017 *J. Am. Chem. Soc.* **139** 17089
[23] Zhang Y, Wang B, Xiao Z, Lu Y, Kamiya T, Uwatoko Y, Kageyama H and Hosono H 2017 *npj Quantum Mater.* **2** 45
[24] Zhang X, Yao Y, Ding S, Bergara A, Li F, Liu Y, Zhou X F and Yang G 2023 *Phys. Rev. B* **107** L100501
[25] Liang Y, Lin X, Wan B, Jia Y, Qian Y, Shao D and Gou H 2025 *npj Comput. Mater.* **11** 220
[26] Ma J, Li Z, Tian H, Yang B, Yuan Y, Li R and Yu R 2024 *Adv. Funct. Mater.* **34** 2316715
[27] Rosner H, Koudela D, Schwarz U, Handstein A, Hanfland M, Opahle I, Koepernik K, Kuz'min M D, Müller K H, Mydosh J A and Richter M 2006 *Nat. Phys.* **2** 469
[28] Bochenek Ł, Rogacki K, Kołodziejczyk A and Cichorek T 2015 *Phys. Rev. B* **91** 235314
[29] Levy O, Hart G L W and Curtarolo S 2010 *Phys. Rev. B* **81** 174106
[30] Moreau J M, Parthé E and Paccard D 1975 *Acta Crystallogr. Sect. B* **31** 747
[31] Podlesnyak A, Ehlers G, Cao H, Matsuda M, Frontzek M, Zaharko O, Kazantsev V A, Gubkin A F and Baranov N V 2013 *Phys. Rev. B* **88** 024117
[32] Kresse G and Hafner J 1994 *Phys. Rev. B* **49** 14251
[33] Blöchl P E 1994 *Phys. Rev. B* **50** 17953

[34] Feng Y, Chen Y, Wang L, Wang J, Chang D, Yuan Y, Wu M, Fu R, Zhang L, Wang Q, Wang K, Guo H and Wang L 2024 *Chin. Phys. Lett.* **41** 063201
[35] Klimeš J, Bowler D R and Michaelides A 2011 *Phys. Rev. B* **83** 195131
[36] Togo A and Tanaka I 2015 *Scr. Mater.* **108** 1
[37] Jung J H, Park C H and Ihm J 2018 *Nano Lett.* **18** 2759
[38] Han W, Wang Z, Guan S, Wei J, Jiang Y, Zeng L, Shen L, Yang D and Wang H 2024 *Appl. Phys. Rev.* **11** 021314
[39] Wan B, Lu Y, Xiao Z, Muraba Y, Kim J, Huang D, Wu L, Gou H, Zhang J and Gao F 2018 *npj Comput. Mater.* **4** 77
[40] Zhang X, Xiao Z, Lei H, Toda Y, Matsuishi S, Kamiya T, Ueda S and Hosono H 2014 *Chem. Mater.* **26** 6638
[41] Lu Y, Li J, Tada T, Toda Y, Ueda S, Yokoyama T, Kitano M and Hosono H 2016 *J. Am. Chem. Soc.* **138** 3970
[42] Zhu Q, Frolov T and Choudhary K 2019 *Matter* **5** 1293
[43] Lu Y, Wang J, Li J, Wu J, Kanno S, Tada T and Hosono H 2018 *Phys. Rev. B* **98** 125128
[44] Meng W, Tian L, Zhou F, Mo Z, Jiao Y, Wang S, Jiang J, Zhang X, Cheng Z, Liu Y, Wang W, Zhang G and Wang X 2025 *Adv. Mater.* **37** 2418904
[45] Wang J, Sui X, Gao S, Duan W, Liu F and Huang B 2019 *Phys. Rev. Lett.* **123** 206402
[46] McRae L M, Radomsky R C, Pawlik J T, Druffel D L, Sundberg J D, Lanetti M G, Donley C L, White K L and Warren S C 2022 *J. Am. Chem. Soc.* **144** 10862
[47] Huang X, Duan L, Zhang Z, Fang C, Chen L, Wang Q, Zhang Y, Shen W, Jia X, Wu L and Wan B 2022 *J. Phys. Chem. C* **126** 20710
[48] Yang J, Wu B, Zhao S, Liu S, Lu J, Li S and Yang J 2024 *Phys. Rev. Appl.* **22** 014017
[49] Zhang S, Guo F, Gao X, Yang M, Huang X, Zhang D, Li X, Zhang Y, Shang Y and Cao A 2024 *Adv. Sci.* **11** 2405880
[50] Song N, Wang Y, Xu G, Pan J, Yuan Z and Wang F 2024 *J. Magn. Magn. Mater.* **599** 172108
[51] Wu D, Mo Z, Li X, Ren X, Shi Z, Li X, Zhang L, Yu X, Peng H, Zeng L and Shan C X 2024 *Appl. Phys. Rev.* **11** 041401
[52] Druffel D L, Woomer A H, Kuntz K L, Pawlik J T and Warren S C 2017 *J. Mater. Chem. C* **5** 11196
[53] Hwang J Y, Lee S Y, Lee K, Regmi B, Lee N, Lim D C, Koo H, Lee W, Kim S G, Kim S W and Lee K H 2025 *Adv. Mater.* **37** 2412956